RESEARCH ARTICLE | JANUARY 23 2026

Self-propelling Leidenfrost ratchet boats FREE

Ivan U. Vakarelski ; Farrukh Kamoliddinov ; Tadd T. Truscott ; Sigurdur T. Thoroddsen

Physics of Fluids 38, 012126 (2026)
https://doi.org/10.1063/5.0304551

Physics of Fluids ARTICLE pubs.aip.org/aip/pof

Self-propelling Leidenfrost ratchet boats

Cite as: Phys. Fluids **38**, 012126 (2026); doi: 10.1063/5.0304551
Submitted: 29 September 2025 · Accepted: 5 January 2026 ·
Published Online: 23 January 2026

Ivan U. Vakarelski,[1,2,a)] Farrukh Kamoliddinov,[1] Tadd T. Truscott,[1] and Sigurdur T. Thoroddsen[1]

AFFILIATIONS

[1]Division of Physical Sciences and Engineering, King Abdullah University of Science and Technology (KAUST), Thuwal 23955-6900, Saudi Arabia

[2]Department of Chemical and Pharmaceutical Engineering, Faculty of Chemistry and Pharmacy, Sofia University, 1 James Bourchier Avenue, 1164 Sofia, Bulgaria

[a)]**Author to whom correspondence should be addressed:** ivakarelski@gmail.com

ABSTRACT

A small liquid droplet placed on an asymmetric ratchet surface heated above the Leidenfrost temperature is known to self-propel. Here, we examine an alternative configuration: a heated macroscopic alumina boat (14 cm long) decorated with asymmetric ratchets and floated in volatile perfluorocarbon liquid. Boats with 1 mm pitch ratchets, heated to 280 °C, showed robust self-propulsion in the expected direction, reaching several centimeters per second and traveling more than one meter. An impulse–momentum balance scaling, derived from Leidenfrost droplet propulsion, predicts boat velocities of the same order but somewhat below experiments, suggesting enhanced efficiency of vapor flow in contact with bulk liquid. Propulsion efficiency depends strongly on ratchet geometry: for small pitches, bottom and sidewall ratchets act synergistically, while at larger pitches, sidewall ratchets reduce thrust by redirecting vapor. Herringbone-patterned ratchets further enhanced propulsion. Towing tests confirmed reduced drag when boats moved with their ratchet orientation, with ∼10% lower drag coefficients compared to smooth boats.

I. INTRODUCTION

When a small liquid droplet is placed on a surface heated to a temperature well above the liquid's boiling point, a stable vapor layer forms between the droplet and the surface. This layer significantly slows the evaporation rate of the droplet, causing it to levitate above the surface, where it becomes highly mobile. This phenomenon is known as the Leidenfrost effect.[1–4] The surface temperature at which this effect occurs for a given liquid depends on the material properties of the surface and can be significantly reduced for water droplets on superhydrophobic surfaces.[5,6]

As first demonstrated by Linke *et al.*, when a liquid droplet is placed on an asymmetric ratchet heated above the Leidenfrost temperature T_L, the rapid movement of the droplet becomes directional along the ratchet.[7] A schematic of a self-propelling Leidenfrost droplet on a ratchet is shown in Fig. 1(a). The mechanism driving this motion is attributed to the rectified vapor flows between the droplet and the surface, which generate a net viscous stress on the droplet along the slope of the ratchet.[8,9] For millimeter-scale ratchets, droplets typically reach velocities of a few centimeters per second. Video 1 and Fig. 1(b) illustrate the self-propelling behavior of a Leidenfrost droplet in the present study. The example features a 280 ° C heated alumina ratchet with a $\lambda = 1$ mm ratchet pitch and a perfluorocarbon liquid (PP1) droplet.

Various studies have been conducted to optimize the droplet movement on ratchets, including investigations into different ratchet dimensions,[10,11] herringbone-ratchet morphologies,[12,13] and the application of superhydrophobic coatings.[14] Most recently, the directional propulsion of Leidenfrost droplets was demonstrated even in symmetric ratchet channels[15] and for various boiling regimes.[16] Beyond the directed movement of liquid droplets, the motion of sublimating solids on ratchets has also been explored,[17,18] as well as the development of sublimation-based heat engines[19] and Leidenfrost heat engines.[20]

Sugioka and Segawa[21] demonstrated a Leidenfrost glider consisting of a light alumina raft (∼2 cm) with a ratcheted bottom that was capable of self-propulsion on shallow water when heated above the Leidenfrost temperature. Because the glider could not float, its operation was restricted to shallow water and a travel time of less than 1 s. Shi *et al.*[22] introduced a dry ice hovercraft that directionally self-propels on room-temperature water via the cold Leidenfrost effect, where propulsion is controlled by a vapor chamber integrated into the bottom of the dry ice slab. Jonas *et al.*[23,24] investigated the drag-reduction effect on submerged ratcheted cylinders free-falling in a fluorocarbon liquid. Various boiling regimes were examined, including single-phase flow, nucleate boiling, and film boiling (Leidenfrost regime), with the cylinder oriented both along and against the ratchet

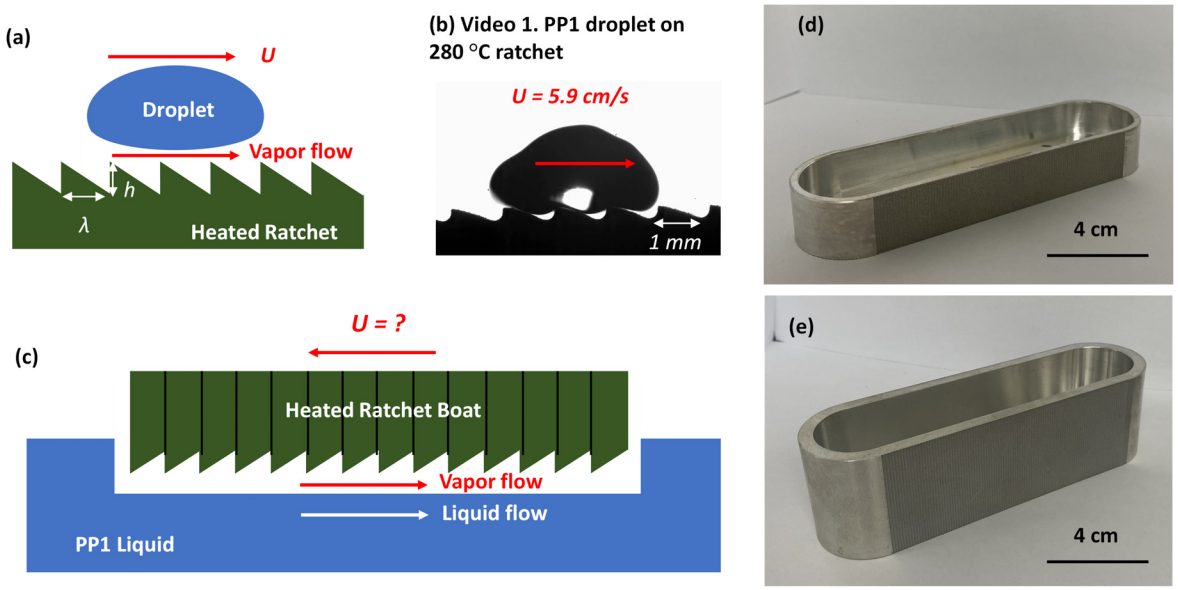

FIG. 1. (a) Schematic of a Leidenfrost ratchet. A liquid droplet is deposited on a hot asymmetric ratchet with tooth pitch length λ and height h. When the ratchet temperature exceeds the Leidenfrost temperature, T_L, the rectified vapor flow propels the droplet in the indicated direction along the ratchet slope. (b) Snapshot from Video 1 showing the directional motion of a PP1 liquid droplet on a heated aluminum ratchet at 280 °C with $\lambda = 1.00$ mm. (c) Schematic of the Leidenfrost ratchet boat. A heated aluminum boat with ratchet patterns on the bottom and sidewalls is floated on PP1 liquid. When the boat temperature exceeds T_L, the rectified vapor flow is expected to propel the boat in the indicated direction against the ratchet slope. Photographs of the shallow (d) and tall (e) aluminum boat types used in the study. Both boats have $\lambda = 1.00$ mm ratchet patterns along the bottom and sidewalls. Exact boat dimensions are provided in supplementary Fig. S1, ratchet profiles in supplementary Fig. S2, and sidewall/bottom ratchet characteristics in Table I.

self-propulsion direction. However, no conclusive evidence was obtained in these studies for drag reduction arising from the Leidenfrost ratchet effect.

Following the Leidenfrost glider work of Sugioka and Segawa[21] and the free-falling ratcheted-cylinder work of Jonas *et al.*,[23,24] the concept of the Leidenfrost ratchet boat introduced herein is illustrated in Fig. 1(c). A macroscopic aluminum boat (14 cm in length) is floated in a liquid pool, with its bottom and side walls decorated with ratchet patterns. This setup creates an alternative configuration of the classic self-propelling droplet on a heated ratchet. If the same mechanism driving the self-propulsion of droplets on a heated ratchet applies to the liquid in contact with the heated ratchet walls, one could expect the boat to self-propel in the direction opposite to the droplet motion on the ratchet, i.e., against the slope of the ratchet [Fig. 1(c)].

To maximize the time that the model boats remain in the Leidenfrost regime, we used a light perfluorocarbon oil, PP1 (perfluoro-2-methylpentane, C_6F_{14}, F2 Chemicals). Light perfluorocarbon oils are chemically inert, thermally resistant, and characterized by a lower boiling point and a much lower heat capacity of vaporization compared to water (approximately 30 times lower). In prior studies, we utilized perfluorocarbon oils to evaluate drag reduction due to Leidenfrost vapor layers sustained on free-falling metallic spheres.[25,26] Recently, these studies were extended to free-falling streamlined aluminum projectiles and towed aluminum boats like the ones used in the present study.[27]

We began our investigation by conducting a set of experiments to test the feasibility of the self-propelling alumina ratchet-boat concept, comparing heated boats with and without ratchets. We then performed multiple trials using boats with ratchets of varying sizes, including those with herringbone-patterned bottoms. Based on the results of these tests, we proposed a phenomenological model describing the vapor flow behavior as a function of ratchet geometry and dimensions and an impulse-momentum balance based scaling that relates the droplet and the boat velocity. Finally, we investigated the effect of ratchets on boat motion in the Leidenfrost regime by towing the boats both along and against the direction of expected ratchet-induced propulsion.

II. EXPERIMENTAL

All alumina boats were custom-fabricated in the KAUST machine workshop using a Mitsubishi FA20S CNC wire Electrical Discharge Machining (EDM) system. Photographs of the two boat types are shown in Figs. 1(d) and 1(e), with exact dimensions provided in supplementary Fig. S1. Both boat types have a total length of 14 cm and a width of 4 cm. The sidewall height was either 2 or 4 cm, corresponding to the "shallow boat" and "tall boat," respectively. The shallow boat has a bottom thickness of 5 mm, sidewall thickness of 3 mm, and a total mass of 110 g. The tall boat has a bottom thickness of 7 mm, sidewall thickness of 5 mm, and a total mass of 240 g. These thicknesses were selected to ensure sufficient buoyancy for stable flotation on PP1 liquid while maximizing the boat mass. Under these conditions, the shallow boat maintains approximately 45% of its height above the PP1 surface, whereas the tall boat maintains about 32% of its height above the surface.

For initial tests, the ratchets on the bottom and sidewalls of the boats had a pitch $\lambda = 1.0$ mm and a height $h = 0.3$ mm [schematic in

TABLE I. Summary of boat configurations used in this study, along with their Leidenfrost-propelled velocities. The first column lists the boat reference codes*. The second column indicates the boat type (shallow or tall). The third and fourth columns specify the ratchet configurations on the bottom and sidewalls, respectively. The fifth and sixth columns report the approximate maximum speed of the boat (cm/s) and the total travel distance (cm) measured experimentally. Values represent averages over at least three runs, with typical deviations indicated *Legend:* The letter A denotes shallow boats, and B denotes tall boats. The next two digits indicate the bottom and sidewall ratchet pitch sizes, respectively, with 0 indicating no ratchet, 1 for $\lambda = 1.00$ mm, 2 for $\lambda = 2.00$ mm, 4 for $\lambda = 4.00$ mm, and 0.5 for $\lambda = 0.50$ mm. The letter H denotes a herringbone-patterned ratchet on the bottom surface.

Boat code*	Shallow/tall	Bottom ratchet λ	Sidewall ratchet λ	Speed (cm/s)	Distance (cm)
A11	Shallow	1.0 mm	1.0 mm	3.1±0.2	100±10
A10	Shallow	No ratchet	1.0 mm	2.1±0.2	50±10
A01	Shallow	1.0 mm	No ratchet	1.6±0.2	25±5
A00	Shallow	No ratchet	No ratchet	0.0±0.2	0.0±0.2
B11	Tall	1.0 mm	1.0 mm	2.3±0.2	90±10
B10	Tall	No ratchet	1.0 mm	1.8±0.2	60±10
B01	Tall	1.0 mm	No ratchet	1.2±0.2	40±5
A.5.5	Shallow	0.5 mm	0.5 mm	2.9±0.2	54±7
A22	Shallow	2.0 mm	2.0 mm	1.5±0.2	20±5
A44	Shallow	4.0 mm	4.0 mm	1.0±0.2	20±5
A04	Shallow	4.0 mm	No ratchet	2.3±0.2	70±10
A0H4	Shallow	4.00 mm herringbone	No ratchet	3.4±0.2	100±10
A4H4	Shallow	4.00 mm herringbone	4.0 mm	2.1±0.2	40±5
A1H4	Shallow	4.00 mm herringbone	1.0 mm	4.3±0.2	120±10

Fig. 1(a), supplementary material Fig. S2(a)]. For reference, we also produced identical boats without any ratchets, as well as boats with ratchets only on the bottom or only on the sidewalls. Specifically, for the shallow boats, we fabricated versions with different ratchet pitches: $\lambda = 0.50$ mm, $\lambda = 2.00$ mm, and $\lambda = 4.00$ mm, keeping $h/\lambda \approx 0.3$. In the case of $\lambda = 4.00$ mm, we produced boats with herringbone-structured bottom ratchets [supplementary material Fig. S2(b)]. All types of ratchet boats produced for this study are summarized in Table I, where each boat type and code are listed for easy reference (see Table I caption for the detailed explanation of the legend for boat reference codes).

The perfluorocarbon liquid (FLUTEC© PP1, F2 Chemicals Ltd.) used in this study is mainly composed of perfluoro-2-methylpentane (C_6F_{14}). It has a boiling point of about 56 ° C, heat of vaporization $H_v = 90\,\mathrm{kJ\,kg^{-1}}$, density $\rho = 1.71\,\mathrm{g\,cm^{-3}}$, dynamic viscosity $\mu = 0.81$mPas, and surface tension $\sigma = 12\mathrm{mNm^{-1}}$. The Leidenfrost temperature of this liquid is $T_L \approx 116$ ° C.[26] The low Leidenfrost temperature and heat of vaporization allow the model boats to maintain Leidenfrost conditions over extended periods. For boats heated to about 280 ° C, the Leidenfrost regime was sustained for 35 ± 5 s for shallow boats and 60 ± 5 s for tall boats. The exact duration depended on boat velocity, with faster-moving boats cooling more quickly. The corresponding average cooling rates are estimated to be $\approx 4.7\,^\circ\mathrm{C\ s^{-1}}$ for the shallow boats and $\approx 2.7\,^\circ\mathrm{C\ s^{-1}}$ for the tall boats.

Experiments were conducted in a liquid channel constructed from clear acrylic, 180 cm in length, 30 cm in width, and 30 cm in height. For the present study, the channel was half-filled with PP1 liquid to a depth of approximately 15 cm. To ensure straight motion, two thin metal guide wires were stretched along the length of the channel, spaced about 4.5 cm apart, and positioned near the liquid surface. Using metal forceps, the preheated boats were carefully released onto the liquid surface within the corridor formed by the wires.

To ensure data reproducibility, all test runs were performed under identical conditions: each boat was pre-heated to 280 ± 5 °C and released from the same position in the tank. Boats were pre-heated for at least 30 min in a temperature-controlled furnace set at 280 °C,[5,25] after which they were rapidly transferred to the test tank. The boat motion was recorded using a high-speed camera (Photron SA-5) at 250 fps, which provides sufficient temporal resolution for accurate determination of the boat velocity. In cases where the boat traveled beyond the camera's field of view, the total travel distance was measured separately. For each boat configuration, the reported values represent averages over at least three repeated runs, and the corresponding variability is indicated in the tables and error bars in figure panels.

As in our previous studies on drag and hydrodynamic regimes for model boats and floating spheres,[27–30] a pulley system with counterweights was used to tow the boats, as schematized in supplementary Fig. S3. A fine fishing line (diameter 0.2 mm) was attached to the front of the boat and routed through the pulley system. A counterweight attached to the other end of the line provided the pulling force, which could be adjusted by varying the mass. To examine the influence of ratchet-induced propulsion on the boats moving in the Leidenfrost regime, tests were conducted with boats preheated to 280 ° C and towed either along or against the ratchet-propulsion direction.

III. RESULTS AND DISCUSSION

A. Proof of concept

As noted in the Introduction, Video 1 demonstrates the self-propulsion of PP1 droplets on the bottom ratchet of the model boat in the case of a $\lambda = 1.00$ mm ratchet. The droplet size is about 3 mm, and the ratchet temperature is 280 °C, well above the PP1 Leidenfrost temperature of about 116 °C. The velocity of the droplets depends on several factors, such as the ratchet temperature and droplet size. In

Video 1 example, the average droplet velocity is about 5.9 cm s^{-1}, and in different tests, the droplet velocity ranged from 3.0 to 6.0 cm s^{-1}, with larger droplets moving faster. A similar range of droplet velocities was recorded for ratchets with $\lambda = 0.50$ mm. However, for ratchets with larger pitches ($\lambda = 2.00$ and 4.00 mm), the PP1 droplets became trapped between the riblets and did not exhibit self-propulsion. This behavior can be attributed to the low surface tension of PP1 and its correspondingly small capillary length. The capillary length, defined as $\lambda_c = \sqrt{\sigma/(\rho g)}$, where g is the gravity, is approximately 0.85 mm for PP1, indicating that when the ratchet pitch significantly exceeds this length scale, the droplets are unable to bridge the grooves and become immobilized.

To test the self-propelled ratchet-boat concept, we conducted a series of runs in which heated boats with or without ratchets were released into the PP1 liquid-filled test channel. In all of these tests, the boats were initially heated to 280 °C before release. Video 2 is a combined video comparing the performance of the shallow boat with the $\lambda = 1.00$ mm ratchet on the bottom and sidewalls (boat A11, top) with the shallow boat without ratchets (boat A00, bottom). While the no-ratchet boat A00 remained in place, the shallow ratchet boat A11 moved steadily in the direction predicted by the ratchet orientation shown in Fig. 1(c).

Figures 2(a)–2(c) show snapshots from Video 2, capturing the boat position at the beginning and toward the end of the video. In this example, the ratchet boat A11 reached a velocity of about 3.0 cm s^{-1} and traveled a distance of about 0.9 m before it cooled below the Leidenfrost temperature and stopped moving. Video 3 provides a top-view visualization of the directional movement of boat A11 along the channel. As seen in the video, the boat moves steadily in a straight line, guided by two parallel wires spanning the length of the channel. Although similar straight motion can occasionally occur without guidance, the use of these wires ensures more consistent and repeatable trajectories across multiple runs. A comparison between cases in which the boat moved straight without guiding wires and those employing wire guidance showed differences in boat speed and travel distance of less than 10%.

Video 4 compares tests conducted with the tall boats, and Figs. 2(d)–2(f) show snapshots from this video capturing the progression of the boat's movement with time. Here, we contrast the performance of a boat with $\lambda = 1.00$ mm ratchets on both the bottom and sidewalls (boat B11, top) with boats carrying ratchets only on the sidewalls (B10, middle), or only on the bottom (B01, bottom). As expected, the best performance was achieved by the fully ratcheted boat (B11), which reached a velocity of about 2.3 cm s^{-1}. This was followed by the sidewall-only ratchet boat (B10), while the bottom-only ratchet boat (B01) performed the worst. Since the wetted sidewall ratchet area is approximately equal to the bottom ratchet area in the tall boat configuration, these results suggest that sidewall ratchets are more effective than bottom ratchets at $\lambda = 1.00$ mm. A similar trend is observed in the shallow boat configuration, where the sidewall-only ratchet boat (A10) also outperforms the bottom-only ratchet boat (A01), despite the sidewall

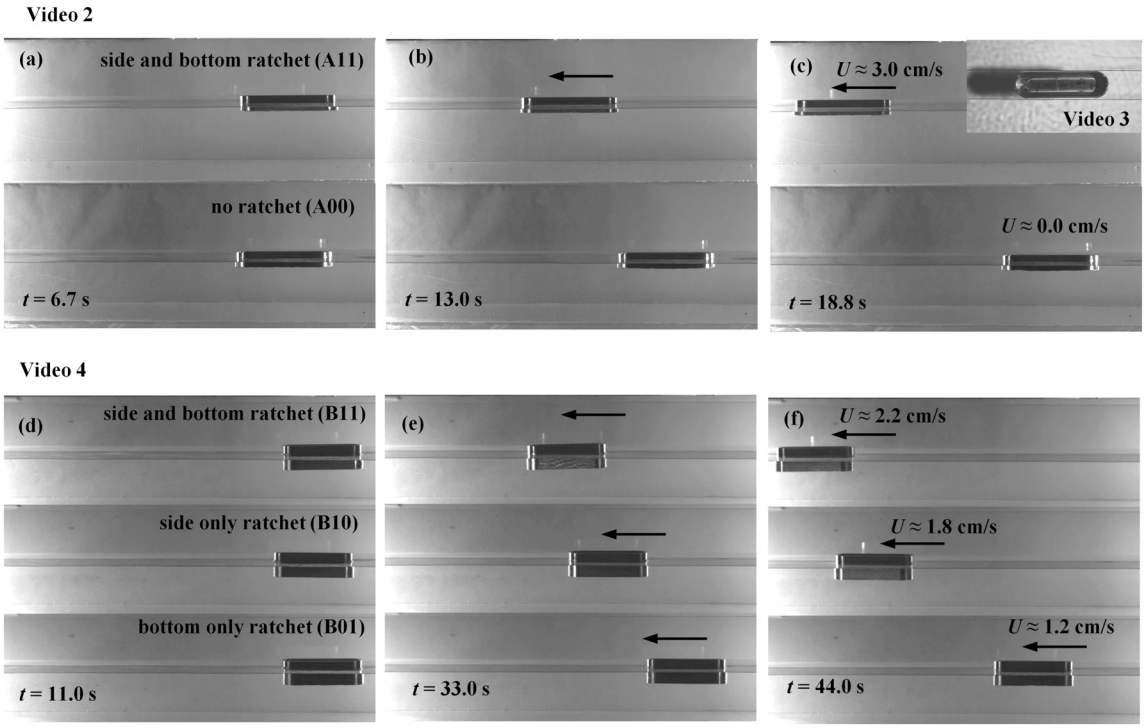

FIG. 2. Snapshots from Video 2 comparing the run of a shallow boat with side and bottom ratchets of $\lambda = 1.00$ mm (top, boat A11) and a no-ratchet boat (bottom, A00) at times (a) 6.7 s, (b) 13.0 s, and (c) 18.8 s. The inset in (c) shows a top-view snapshot from Video 3 of boat A11 in motion. Snapshots from Video 4 compare the run of a tall boat with side and bottom $\lambda = 1.00$ mm ratchets (top, boat B11), a boat with side-only ratchets (middle, B10), and a boat with bottom-only ratchets (bottom, B01) at times (d) 11.0 s, (e) 33.0 s, and (f) 44.0 s. All boats start from approximately the same position at the same time.

ratchet wet area being about 50% smaller than the bottom ratchet area (see Table I).

We note that while the Leidenfrost state is maintained for a longer time on the tall boat than on the shallow boat, the total travel distance is similar in both cases due to the slower acceleration of the tall boat. Because the tall boat is also heavier, this observation suggests comparable efficiency in terms of heat dissipation per unit distance traveled per unit mass.

To make this observation quantitative, we estimate the heat dissipated by the boat during propulsion as $J = C_a m_B (T_B - T_L)$, where $C_a \approx 0.9\,\mathrm{kJ\,kg^{-1}\,^\circ C^{-1}}$ is the specific heat capacity of aluminum, m_B is the boat mass, T_B the initial boat temperature, and T_L the Leidenfrost temperature of PP1. Normalizing by the travel distance l_B and mass gives

$$\frac{J}{l_B m_B} = \frac{C_a (T_B - T_L)}{l_B}. \tag{1}$$

Using $T_B - T_L \approx 164\,^\circ\mathrm{C}$ and a representative travel distance of $l_B \approx 1.0$ m for both shallow and tall boats give

$$\frac{J}{l_B m_B} \approx 1.5\,\mathrm{kJ\,m^{-1}\,kg^{-1}} \tag{2}$$

for both boat types. This estimate supports the conclusion that shallow and tall boats exhibit comparable thermal efficiency despite differences in mass, acceleration, and cooling time.

Our proof-of-concept tests shows that the same mechanism of rectified vapor shear stress that propels Leidenfrost droplets at characteristic Reynolds numbers of $\mathrm{Re} \sim 10^2$ can generate macroscopic thrust on boats operating at $\mathrm{Re} \sim 10^4$, i.e., two orders of magnitude larger. For droplets, the Reynolds number is estimated as $Re = U_d D \rho_{air}/\mu_{air}$, where U_d is the droplet velocity, D is the droplet diameter, ρ_{air} is the air density, and μ_{air} is the air dynamic viscosity. For the boats, the characteristic Reynolds number is $Re = U_B L \rho/\mu$, where U_B is the boat velocity, L is the wetted hull length, and ρ μ are the density and dynamic viscosity of the PP1 liquid. Here, we use the properties of the fluid in which the object moves, thereby providing the drag. This comparison highlights the regime change from viscous–inertial droplet motion to predominantly inertial macroscopic hydrodynamic behavior.

To estimate the relative importance of viscous stresses in our system, we form the Capillary number, defined as $\mathrm{Ca} = \mu U/\sigma$. Taking a representative velocity of $U \approx 3\,\mathrm{cm\,s^{-1}}$, we obtain $\mathrm{Ca} \sim 2 \times 10^{-3}$. This small-to-moderate Capillary number indicates that capillary forces dominate over viscous stresses in both droplet and boat configurations.

The boat velocities observed in these proof-of-concept tests (2.0–3.0 $\mathrm{cm\,s^{-1}}$) are somewhat lower but still comparable to the velocities of PP1 Leidenfrost droplets on ratchets (3.0–6.0 $\mathrm{cm\,s^{-1}}$). This similarity indicates that related mechanisms underlie both droplet propulsion on ratchets and boat propulsion along the liquid surface. In Sec. III D, "Impulse-momentum balance," we develop a scaling argument that links droplet and boat velocities, providing further insight into the underlying propulsion mechanism.

B. Ratchets of different sizes and with herringbone pattern

Next, we compare the performance of boats decorated with various ratchet configurations. In these tests, we used identical shallow boats equipped with bottom and sidewall ratchets having pitches of $\lambda = 0.50$, 1.00, 2.00, and 4.00 mm (Video 5), as well as boats featuring bottom herringbone-patterned ratchets with $\lambda = 4.00$ mm (Video 6). In all cases, the boats were heated to 280 °C before being released into the channel. Figure 3(a) shows an example of the boat velocity as a function of time, extracted from Video 5 for the shallow boat with $\lambda = 1.00$ mm ratchets on the sidewalls and bottom (A11). Figure 3(b) presents a corresponding example extracted from Video 4 for the tall boat with $\lambda = 1.00$ mm ratchets on the sidewalls and bottom (B11). However, because the velocity evolution is often irregular, boat performance is more conveniently compared in terms of maximum velocity and total travel distance recorded during each test.

Video 5 compares the performance of boats with straight ratchets on both the sidewalls and bottom, but with different pitches (from top to bottom): $\lambda = 0.50$ mm (boat A.5.5), $\lambda = 1.00$ mm (boat A11), $\lambda = 2.00$ mm (boat A22), and $\lambda = 4.00$ mm (boat A44). The diagram in Fig. 4 summarizes the boat performance in terms of maximum velocity and total travel distance. It is evident that the $\lambda = 1.00$ mm ratchet boat (A11) exhibits the best performance, followed by the $\lambda = 0.50$ mm boat (A.5.5). In contrast, the $\lambda = 2.00$ and 4.00 mm

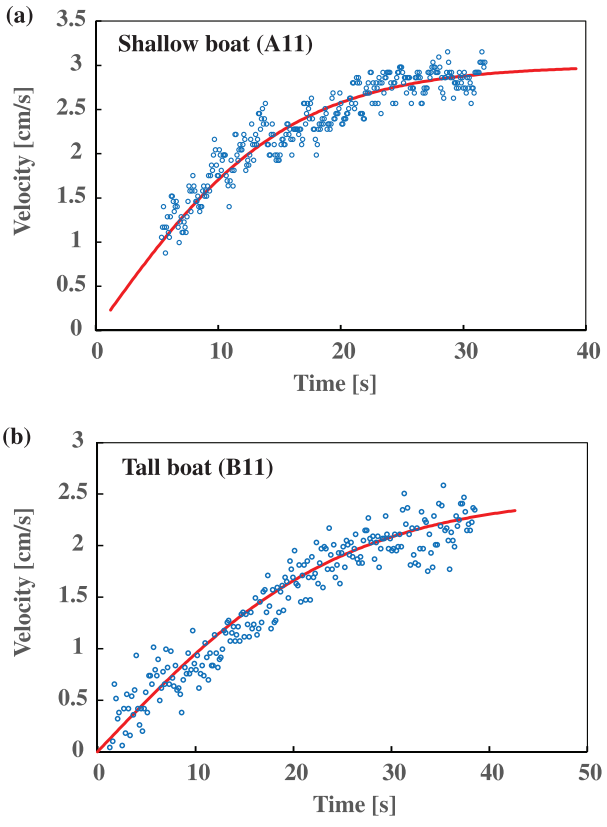

FIG. 3. Examples of boat velocity as a function of time. (a) Data extracted from Video 5 for the shallow boat with side and bottom ratchets of pitch $\lambda = 1$ mm (second from top, boat A11). (b) Data extracted from Video 4 for the tall boat with side and bottom ratchets of pitch $\lambda = 1$ mm (top, boat B11). Dots represent the raw data, while the solid red line is a fit of Eq. (A4) using the best-fit parameters $U_T = 3.0$ m/s and $\tau = 15.5$ s for the shallow boat (a) and $U_T = 2.5$ m/s $\tau = 25.0$ s for the tall boat (b).

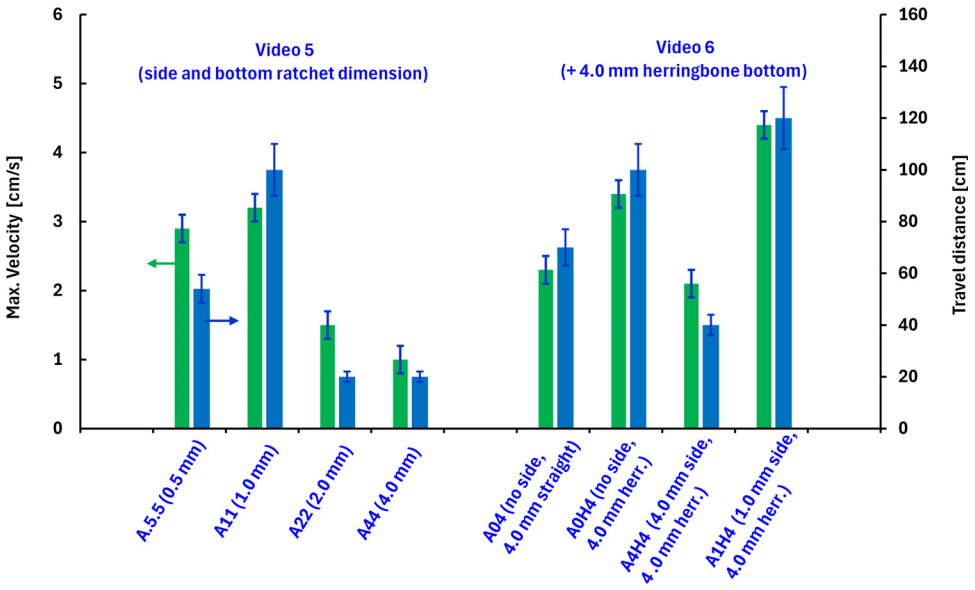

FIG. 4. Performance of various ratchet-configured boats, shown by the approximate maximum velocity (green bars, left vertical axis) and total travel distance (blue bars, right vertical axis). Boat types are labeled on the horizontal axis using their reference codes. The first group of four boats corresponds to configurations compared in Video 5, which examines the effect of different ratchet sizes for straight ratchets on both the sidewalls and bottom (boats A.5.5, A11, A22, and A44). The second group of four boats corresponds to Video 6, comparing boats with $\lambda = 4.0$ mm bottom ratchets of either straight or herringbone geometry, and with or without sidewall ratchets (boats A04, A0H4, A4H4, and A1H4). Each data column represents the average of at least three experimental runs, with error bars indicating the typical spread across repeated measurements.

boats take longer to initiate movement, travel more slowly, and ultimately move significantly shorter distances. The possible reason for the difference in the smaller and larger pitch ratchets performance observed here will be discussed in Sec. III C.

Due to manufacturing constraints, the only herringbone ratchet structure considered here was a bottom ratchet with $\lambda = 4.00$ mm [supplementary material, Figs. S2(b) and S2(c)]. The following boats were produced with this bottom herringbone pattern: a boat without any sidewall ratchets (A0H4), a boat with $\lambda = 4.00$ mm sidewall ratchets (A4H4), and a boat with $\lambda = 1.00$ mm sidewall ratchets (A1H4). All sidewall ratchets were straight in the vertical direction. Video 6 compares the performance of these boats, including also a boat with no sidewall ratchets and a $\lambda = 4.00$ mm straight bottom ratchet (A04). Figure 4 summarizes the approximate maximum velocity and travel distance for these four boats, which are compared in Video 6 (from top to bottom: A04, A0H4, A4H4, and A1H4).

The first notable observation from Video 6 and Fig. 4 is that among boats without sidewall ratchets, the herringbone-pattern boat A0H4 outperforms the straight-ratchet boat A04. Second, adding $\lambda = 4.00$ mm sidewall ratchets reduces performance for both the straight (A44) and herringbone (A4H4) bottom-ratchet boats, as their performance drops significantly compared to the corresponding no-sidewall-ratchet boats (A04 and A0H4, respectively). Interestingly, the $\lambda = 4.00$ mm straight bottom-ratchet boat without sidewall ratchets (A04) performs much better than the $\lambda = 1.00$ mm bottom-only ratchet boat (A01), and the $\lambda = 4.00$ mm herringbone bottom-ratchet boat without sidewall ratchets (A0H4) performs comparably to the fully ratcheted $\lambda = 1.00$ mm boat (A11). Finally, unlike the $\lambda = 4.00$ mm sidewall ratchets, adding $\lambda = 1.00$ mm sidewall ratchets to the herringbone bottom ratchet (A1H4) further enhances performance, making it one of the best-performing configurations among all tested shallow boats, reaching velocity of about 4.3 cm s^{-1} and traveled a distance of about 1.2 m.

C. Mechanism of boat propulsion

Based on the performance of the various ratcheted boats, we propose general mechanisms for their propulsion, which are schematically illustrated in Fig. 5. For clarity, we primarily consider the vapor flow induced by the ratchets on the bottom surface of the boat, though similar principles are expected to apply to the ratcheted sidewalls that are in contact with the liquid.

During the self-propelled motion of the heated boats operating in the Leidenfrost or film-boiling regime, a stable vapor layer separates the boat surface from the liquid. The direction of vapor flow determines the viscous stress exerted on the surrounding liquid, thereby generating thrust in the direction opposite to the vapor flow. In the case of a non-ratcheted (flat-bottom and walls) boat, as schematized in Fig. 5(a), the vapor flow is symmetric, resulting in no net force acting on the boat.

We hypothesize two preferential directions for vapor flow when ratchets are present. One is along the slope of the ratchets, driven by the same rectified flow mechanism responsible for the propulsion of Leidenfrost droplets [Figs. 1(a)–1(c)]. The second is along the grooves of the ratchets. Due to symmetry, vapor flow along the grooves in straight-ratchet geometries produces no net force and, thus, does not contribute to propulsion. As illustrated in Figs. 5(b) and 5(c) and supported by observations in Video 5, we propose that for smaller-pitch ratchets ($\lambda = 0.50$ and 1.00 mm) the dominant vapor flow for both bottom and sidewall ratchets is directed along the ratchet slope

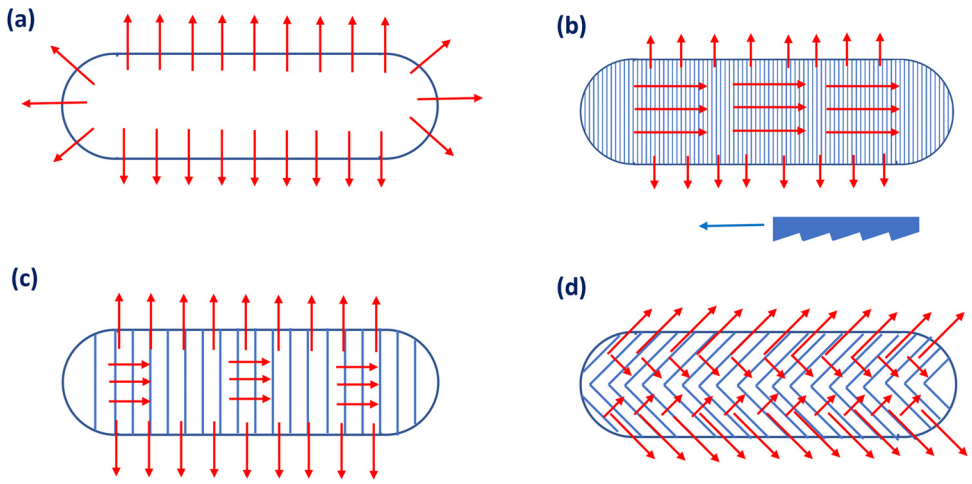

FIG. 5. Schematics illustrating the anticipated vapor flow directions beneath the boat bottom for various ratchet configurations: (a) flat-bottom boat with symmetric vapor flow and no net propulsion; (b) boat with small-pitch ratchets, where vapor is rectified along the ratchet slope, resulting in effective propulsion. The inset shows ratchet angles and travel directions for panels (b)–(d) (see also Fig. 6); (c) boat with large-pitch ratchets, where vapor predominantly flows along the ratchet grooves, reducing propulsion efficiency; and (d) boat with herringbone-patterned ratchets, where vapor flows are directed at an angle to the boat's longitudinal axis, enhancing propulsion.

[Fig. 5(b)], resulting in efficient propulsion. In contrast, for larger-pitch ratchets ($\lambda = 2.00$ and 4.00 mm), the presence of sidewall ratchets appears to enhance lateral vapor drainage along the grooves [Fig. 5(c)], thereby redirecting flow away from the slope and reducing propulsion efficiency.

The vapor flow along the bottom ratchet as proposed in Fig. 5(c) is applicable only when larger-pitch ratchets are present on the sidewalls. Interestingly, for bottom-only ratchet configurations, boats with larger-pitch $\lambda = 4.00$ mm ratchets (A04) perform better than those with $\lambda = 1.00$ mm ratchets (A01). As noted earlier for droplets, the maximum ratchet pitch enabling effective propulsion is limited by the PP1 capillary length, $\lambda_C \approx 0.85$ mm. However, no such limitation applies to the boats: efficient propulsion was observed even with bottom–surface ratchets of pitch 4 mm, far exceeding the capillary length. Keep in mind that the direction of gravity is inverted in the two geometries. For the drop, it pulls against the bottom free surface, trying to pull it down, while for the ratchet, gravity tries to make bottom vapor layer flat, stabilizing it. The higher efficiency of larger-pitch bottom ratchets in the absence of sidewall ratchets is not yet fully understood, likely reflecting complex vapor dynamics that will require detailed theoretical or numerical analysis.

The bottom-only $\lambda = 4.00$ mm herringbone ratchet demonstrates even greater effectiveness than the corresponding straight $\lambda = 4.00$ mm bottom-only ratchet (Video 6). Enhanced performance in this design may be attributed to the 45° orientation of the riblets relative to the boat's longitudinal axis, which likely redirects vapor flow to produce a net component along the motion direction, generating more effective thrust, as illustrated schematically in Fig. 5(d).

D. Impulse-momentum balance

Next, to evaluate whether the propulsion of small-pitch ratcheted boats is governed by the same rectified vapor–flow mechanism as Leidenfrost droplets, we employ an impulse–momentum balance. A schematic of this balance is shown in Fig. 6, highlighting how droplet and boat velocities may be scaled relative to one another.

For a Leidenfrost droplet moving over a ratchet, the momentum is $p_d = m_d U_d$, where m_d and U_d are the droplet mass and speed,

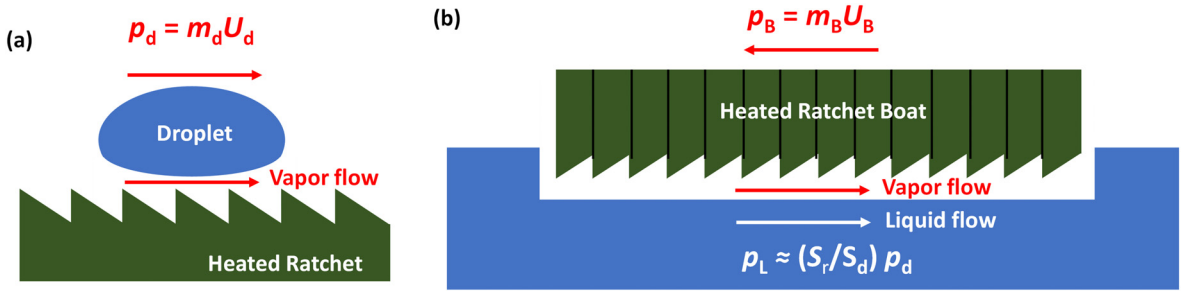

FIG. 6. Schematics illustrating the impulse–momentum balance. (a) Droplet on a heated ratchet with momentum $p_d = m_d U_d$, directed along the ratchet slope. (b) Heated ratchet boat with momentum $p_B = m_B U_B$. The impulse transferred from the ratchet to the surrounding liquid is assumed to scale with the droplet case as (S_r/S_d), i.e., $p_L \approx (S_r/S_d) p_d$, also directed along the ratchet slope. Neglecting drag forces, this balance leads to the scaling relation in Eq. (5) between boat and droplet velocities.

respectively. For a boat, the momentum is $p_B = m_B U_B$, with m_B and U_B being the boat mass and speed.

Unlike droplets, the boat experiences appreciable hydrodynamic drag during acceleration. The drag impulse accumulated over a characteristic acceleration time τ is $p_D = \frac{1}{2} C_D \rho A U_B^2 \tau$, where C_D is the drag coefficient, ρ is the liquid density, A is a wetted surface area of the boat, and τ is the time over which the boat approaches its terminal velocity. Thus, the total impulse required to accelerate the boat to speed U_B, including drag losses $F_D \tau$, is

$$p_{BD} = m_B U_B + \frac{1}{2} C_D \rho A U_B^2 \tau. \tag{3}$$

If the rectified vapor shear imparts the same impulse per unit ratchet area to both droplets and boats (i.e., a comparable mean tangential vapor stress acting over a similar interaction time), then the total vapor impulse received by the boat scales with the ratio of wetted ratchet areas. If S_r is the boat's wetted ratchet area and S_d the droplet contact area, the impulses satisfy

$$m_B U_B + \frac{1}{2} C_D \rho A U_B^2 \tau \approx \left(\frac{S_r}{S_d}\right) m_d U_d. \tag{4}$$

If one neglects drag during acceleration, Eq. (2) reduces to the simplified order-of-magnitude scaling,

$$U_B \approx \left(\frac{m_d}{m_B}\right)\left(\frac{S_r}{S_d}\right) U_d. \tag{5}$$

From the droplet example in Video 1, $D \sim 3.0$ mm, we estimate $m_d \approx 0.014$ g, $S_d \approx 0.07$ cm^2, and $U_d \approx 5.9$ cm s^{-1}. For the shallow boat ($m_B = 110$ g and $S_r \approx 74$ cm^2), Eq. (5) gives $U_B \approx 0.7$ cm s^{-1}. For the tall boat ($m_B = 240$ g and $S_r \approx 108$ cm^2), the estimate is $U_B \approx 0.5$ cm s^{-1}. Using instead data for smaller droplets of diameter, $D \sim 2$ mm moving at $U_d \approx 3.0$ cm s^{-1} yields predicted velocities of $U_B \approx 0.3$ cm s^{-1} for the shallow and $U_B \approx 0.2$ cm s^{-1} for the tall boat.

Although these predicted velocities are of the correct order of magnitude, they remain below the experimentally observed 2.0–3.0 cm s^{-1} achieved in our proof-of-concept tests. Since hydrodynamic drag was neglected in this simplified scaling, this discrepancy suggests that rectified vapor flow beneath a bulk liquid may generate thrust more efficiently than in the droplet-on-ratchet case.

To further refine our scaling by accounting for boat drag, the principal unknown in Eq. (4) is the drag coefficient C_D during the acceleration phase. One approach to estimate C_D is to fit the experimental velocity–vs–time data using the boat equation of motion. The Appendix details this procedure and provides examples based on the data shown in Fig. 3(a) for the shallow boat and Fig. 3(b) for the tall boat. For the shallow boat [A11, Fig. 3(a)], this method yields $C_D \approx 0.02$. Using this value gives a drag impulse of $p_D \approx 3.1 \times 10^{-3}$Ns, which is comparable to the boat momentum $p_B \approx 3.2 \times 10^{-3}$Ns at $U = 3.0$ cm s^{-1}. For the tall boat [B11, Fig. 3(b)], the fit gives $C_D \approx 0.04$. The corresponding drag impulse is $p_D \approx 4.4 \times 10^{-3}$Ns, which is likewise comparable to the boat momentum $p_B \approx 5.2 \times 10^{-3}$Ns at $U = 2.2$ cm s^{-1}. However, including drag and using the full scaling of Eq. (4), rather than the simplified form of Eq. (5), produces only modest corrections to the predicted boat speeds: from $U_B \approx 0.75$ cm s^{-1} [Eq. (5)] to $U_B \approx 0.62$ cm s^{-1} [Eq. (4)] for the shallow boat, and from $U_B \approx 0.50$ cm s^{-1} [Eq. (5)] to $U_B \approx 0.43$ cm s^{-1} [Eq. (4)] for the tall boat. These examples indicate that, for order-of-magnitude purposes, the simplified scaling of Eq. (5) remains a reasonable approximation.

In summary, although the propulsion mechanism of ratcheted boats is fundamentally related to Leidenfrost droplet propulsion, the surrounding vapor dynamics are considerably more complex. The impulse–momentum balance scaling suggests that, under the base configuration, boat propulsion is more effective than in the droplet case. However, the correspondence between droplet and boat behavior is not straightforward: for instance, larger-pitch bottom-only ratchets unexpectedly outperform smaller-pitch ones, a trend not predicted by droplet dynamics. Moreover, interactions between bottom and sidewall ratchets can be either synergistic or counterproductive, depending on geometry. These findings underscore the intricate nature of vapor-mediated propulsion in macroscopic systems and highlight the need for complementary experimental, theoretical, and computational studies to fully resolve the mechanisms and optimize ratchet designs. An important part of the future work will be to confirm the proposed vapor-flow mechanisms illustrated in Figs. 5 and 6, using flow-visualization techniques, such as Schlieren imaging or tracer-based methods, where the motion of the heated propulsive liquid could be traced.

E. Effect of ratchets on moving boats

Finally, we investigate the effect of ratchets on boats already moving in the Leidenfrost regime. This is accomplished by comparing the velocity and drag of boats towed in the direction in which the ratchet is expected to reduce drag, referred to as the "along-propulsion" direction, and in the opposite direction, where the ratchet is expected to increase drag, referred to as the "against-propulsion" direction.

The experimental setup used to tow the boats in the PP1 liquid tank with a counterweight–pulley system is shown in supplementary Fig. S3. In a recent study, we employed the same setup to tow alumina boats (identical in shape to the tall boats used here, but without ratchets) to investigate the influence of the Leidenfrost vapor layer on drag.[27] While free-falling spheres in the Leidenfrost regime can exhibit drag reductions of up to an order of magnitude, due to delayed separation and smaller wakes, a much smaller difference was found between the drag on unheated (room-temperature) and heated (280 °C) alumina boats towed in PP1.[25–27] This suggests that skin-friction drag, which dominates for streamlined bodies like boats, is much less sensitive to the presence of a vapor layer compared to form drag, which dominates for bluff bodies such as spheres.

In the present tests, we used the tall boat with $\lambda = 1.00$ mm ratchets on both the bottom and sidewalls (boat B11). In all experiments, the boat was preheated to approximately 280 °C, which was sufficient to maintain the Leidenfrost regime for the entire duration of the test. Figure 7(a) presents the velocity of the towed ratcheted boat as a function of towing force, for both the along- and against-propulsion directions. Videos 7 and 8 show parallel examples of the boat being towed along (top) and against (bottom) the ratchet direction at towing forces of about 18 and 38 mN, respectively. As shown in Fig. 7(a) and supported by Videos 7 and 8, the boat towed in the along-propulsion direction consistently exhibits higher velocity across the entire range of towing forces. The average velocity difference between the two cases is approximately 2 cm s^{-1}, which is comparable to the self-propulsion velocity of the ratcheted boats.

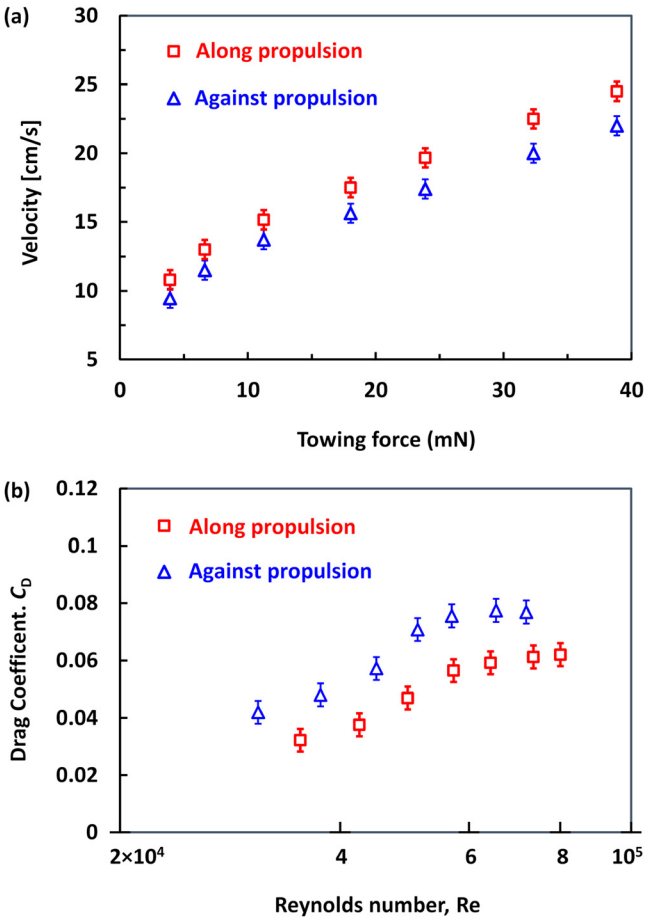

FIG. 7. (a) Velocity dependence on the towing force for the tall boat with sidewall and bottom $\lambda = 1.00$ mm ratchets (boat B11) when towed in the Leidenfrost regime along (squares) or against (triangles) the ratchet-propulsion direction. (b) The same data plotted as drag coefficient, C_D, as a function of the Reynolds number, *Re*. Each data point represents the average of at least three experimental runs, with error bars indicating the typical spread across repeated measurements.

Figure 7(b) presents the same data as Fig. 7(a), but in terms of the drag coefficient, defined as $C_D = 2F_D/(\rho U^2 A)$, plotted against the Reynolds number, $Re = UL\rho/\mu$, where μ is the dynamic viscosity of PP1, ρ is the fluid density, U is the boat velocity, L is a characteristic length scale, and A is a characteristic surface area. For constant speed, the drag force F_D is taken to be equal to the applied towing force F_{Tow}. For these model boats, it is convenient to define the characteristic length as the wetted length of the boat hull, $L = L_{\mathrm{wt}}$, and the characteristic area as the wetted surface area, $A = A_{\mathrm{wt}}$. For the boats used in these experiments, these values are approximately $L_{\mathrm{wt}} \approx 16.3$ cm and $A_{\mathrm{wt}} \approx 128\ \mathrm{cm}^2$.

As seen in Fig. 7(b), the drag coefficient for boats towed in the along-propulsion direction is approximately 20% lower than when towed in the against-propulsion direction. This reduction can also be interpreted as a $\sim 10\%$ decrease in drag coefficient for ratcheted boats moving in the along-propulsion direction, when compared to non-ratcheted boats operating under Leidenfrost conditions within the same Reynolds number range. This magnitude of drag reduction is comparable to that achieved with other passive drag-reduction strategies, including surface microstructuring,[31] lubricating coatings,[32] and the use of superhydrophobic surfaces that sustain thin air layers.[28,33]

IV. CONCLUSIONS

We have demonstrated that heated alumina boats with asymmetric ratchets can achieve self-propulsion in the Leidenfrost regime, a macroscopic analogue of the well-known propulsion of Leidenfrost droplets on ratchets.[7–9] Boats preheated to 280 °C reached velocities of several centimeters per second and traveled distances exceeding one meter before cooling to the Leidenfrost temperature (~ 116 °C).

The propulsion efficiency was found to depend strongly on ratchet geometry. Sidewall ratchets enhanced performance for small-pitch designs ($\lambda = 1.00$ mm) but suppressed it at larger pitches ($\lambda = 4.00$ mm), while bottom-only herringbone ratchets at $\lambda = 4.00$ mm produced the largest thrust. Towing experiments confirmed that this propulsion reduces drag by about 10% within the tested Reynolds number range.

A simple impulse–momentum balance scaling predicts boat velocities of the same order of magnitude as droplets, but somewhat below experimental values, suggesting that rectified vapor flow in contact with a bulk liquid may be more efficient than in the droplet-on-ratchet case. While the fundamental mechanism is shared, the interplay between bottom and sidewall ratchets, as well as the unexpected performance of larger-pitch geometries, highlights the greater complexity of vapor dynamics in macroscopic systems. These findings motivate further experimental, theoretical, and computational studies to optimize Leidenfrost ratchet propulsion at larger scales.

SUPPLEMENTARY MATERIAL

See the supplementary material for additional figures, including boat dimensions and ratchet layouts (Fig. S1), ratchet profiles and herringbone geometry (Fig. S2), the towing setup (Fig. S3), and the description of the videos.

ACKNOWLEDGMENTS

The work was supported by the King Abdullah University of Science and Technology (KAUST) under Grant Nos. URF/1/2126-01-01, URF/1/3727-01-01, and BAS/1/1352-01-01. I.U.V. acknowledges the financial support of Project CoC "Smart Mechatronics, Eco- and Energy Saving Systems and Technologies," No. BG16RFPR002-1.014-0005, funded by the European Regional Development Fund under the Operational Program "Scientific Research, Innovation and Digitization for Smart Transformation 2021-2027."

AUTHOR DECLARATIONS

Conflict of Interest

The authors have no conflicts to disclose.

Author Contributions

Ivan U. Vakarelski: Conceptualization (lead); Data curation (equal); Formal analysis (equal); Investigation (equal); Writing – original draft (lead); Writing – review & editing (equal). **Farrukh Kamoliddinov:**

Conceptualization (equal); Data curation (equal); Investigation (equal); Writing – review & editing (equal). **Tadd T. Truscott:** Formal analysis (equal); Funding acquisition (equal); Supervision (equal); Writing – review & editing (equal). **Sigurdur T. Thoroddsen:** Conceptualization (equal); Formal analysis (equal); Funding acquisition (equal); Supervision (equal); Writing – review & editing (equal).

DATA AVAILABILITY

The data that support the findings of this study are available from the corresponding author upon reasonable request.

NOMENCLATURE

A	Wetted surface area of the boat (m^2)
C_D	Hydrodynamic drag coefficient
Ca	Capillary number
F_D	Hydrodynamic drag force (N)
F_T	Propulsive trust force (N)
F_{Tow}	Towing force (N)
J	Heat dissipation (J)
m_B	Mass of the boat (kg)
m_d	Mass of a Leidenfrost droplet (kg)
p_B	Boat momentum, $p_B = m_B U_B$ (kg m/s)
p_D	Drag-related momentum loss (kg m/s)
p_d	Droplet momentum, $p_d = m_d U_d$ (kg m/s)
S_d	Droplet contact area (m^2)
S_r	Wetted ratchet area on the boat (m^2)
T_B	Boat temperature (°C)
T_L	Leidenfrost temperature (°C)
t	Time (s)
$U(t)$	Instantaneous boat velocity (m/s)
U_B	Boat velocity (m/s)
U_d	Leidenfrost droplet velocity (m/s)
U_T	Boat terminal velocity (m/s)
λ	ratchet pitch (m)
λ_c	capillary length (m)
μ	Dynamic viscosity (Pa s)
ρ	Density of the liquid bath (kg/m^3)
σ	Surface tension (N/m^{-1})
τ	Characteristic acceleration time (s)

APPENDIX: EQUATION OF THE BOAT MOTION

Here, we detail how the experimental velocity–vs–time data, when fit with a simplified equation of motion, can be used to determine the effective drag coefficient during boat acceleration together with the vapor thrust force acting on the boat. The equation of motion accounting for the vapor thrust force F_T and the hydrodynamic drag force $F_D = \frac{1}{2} C_D \rho A U^2$ is

$$m_B \frac{dU}{dt} = F_T - \frac{1}{2} C_D \rho A U^2. \tag{A1}$$

Here, we ignore the added (virtual) mass force, which for a streamlined boat is expected to be small compared to the thrust and drag forces.

At steady state ($dU/dt = 0$), Eq. (A1) gives

$$F_T = \frac{1}{2} C_D \rho A U_T^2. \tag{A2}$$

And, therefore, the terminal velocity is

$$U_T = \sqrt{\frac{2F_T}{C_D \rho A}}. \tag{A3}$$

For a constant drag coefficient C_D, Eq. (A1) can be solved analytically using partial fractions. With the initial condition $U(0) = 0$, the solution is[34]

$$U(t) = U_T \tanh\left(\frac{t}{\tau}\right) = U_T \left(\frac{1 - e^{-2t/\tau}}{1 + e^{-2t/\tau}}\right), \tag{A4}$$

where the characteristic acceleration time is

$$\tau = \frac{m_B U_T}{F_T}. \tag{A5}$$

By fitting the experimental velocity–time data with Eq. (A4), U_T and τ can be extracted as the best-fit parameters. The thrust force and drag coefficient can then be computed as

$$F_T = \frac{m_B U_T}{\tau}, \tag{A6}$$

$$C_D = \frac{2F_T}{\rho A U_T^2}. \tag{A7}$$

Applying Eq. (A4) to the velocity–time data for the shallow boat (A11) in Fig. 3(a) yields a best-fit terminal velocity of $U_T \approx 3.0\,\text{cm/s}$ and a characteristic time $\tau \approx 15.5\,\text{s}$. Using Eqs. (A6) and (A7), we obtain a thrust force of $F_T \approx 2.1 \times 10^{-4}\,\text{N}$ and a drag coefficient of $C_D \approx 0.023$.

Applying the same analysis to the tall boat (B11) in Fig. 3(b) gives a best-fit terminal velocity of $U_T \approx 2.5\,\text{cm/s}$ and a characteristic time $\tau \approx 25.0\,\text{s}$. From Eqs. (A6) and (A7), this case yields $F_T \approx 2.4 \times 10^{-4}\,\text{N}$ and a drag coefficient of $C_D \approx 0.036$.

These values are used in the main text to estimate the contribution of the drag-related impulse. We also note the excellent agreement between the drag coefficients obtained from fitting the boat acceleration data and those measured in the towing experiments [Fig. 7(b)], which supports the consistency of our model.

REFERENCES

[1] J. G. Leidenfrost, *De Aquae Communis Nonnullis Qualitatibus Tractatus* (Ovenius, 1756).
[2] A.-L. Biance, C. Clanet, and D. Quéré, "Leidenfrost drops," Phys. Fluids **15**, 1632–1637 (2003).
[3] D. Quéré, "Leidenfrost dynamics," Annu. Rev. Fluid Mech. **45**, 197–215 (2013).
[4] H. Gu, B. Ji, J. Zhang, Y. Zhu, R. Tao, J. Li, and W. Zuankai, "Leidenfrost effect on engineered surfaces," Adv. Funct. Mater. **36**, 2423686 (2025).
[5] I. U. Vakarelski, N. A. Patankar, J. O. Marston, D. Y. Chan, and S. T. Thoroddsen, "Stabilization of Leidenfrost vapour layer by textured superhydrophobic surfaces," Nature **489**, 274–277 (2012).
[6] P. Bourrianne, C. Lv, and D. Quéré, "The cold Leidenfrost regime," Sci. Adv. **5**, eaaw0304 (2019).
[7] H. Linke, B. Alemán, L. Melling, M. Taormina, M. Francis, C. Dow-Hygelund, V. Narayanan, R. Taylor, and A. Stout, "Self-propelled Leidenfrost droplets," Phys. Rev. Lett. **96**, 154502 (2006).
[8] G. Dupeux, M. Le Merrer, G. Lagubeau, C. Clanet, S. Hardt, and D. Quéré, "Viscous mechanism for Leidenfrost propulsion on a ratchet," Europhys. Lett. **96**, 58001 (2011).

[9]Á. G. Marín, D. Arnaldo del Cerro, G. R. Römer, B. Pathiraj, A. Huis in 't Veld, and D. Lohse, "Capillary droplets on Leidenfrost micro-ratchets," Phys. Fluids **24**, 122001 (2012).
[10]J. T. Ok, J. Choi, E. Brown, and S. Park, "Effect of different fluids on rectified motion of Leidenfrost droplets on micro/sub-micron ratchets," Microelectron. Eng. **158**, 130–134 (2016).
[11]J. M. Arter, D. J. Cleaver, K. Takashina, and A. T. Rhead, "Self-propelling Leidenfrost droplets on a variable topography surface," Appl. Phys. Lett. **113**, 243704 (2018).
[12]D. Soto, G. Lagubeau, C. Clanet, and D. Quéré, "Surfing on a herringbone," Phys. Rev. Fluids **1**, 013902 (2016).
[13]L. E. Dodd, P. Agrawal, M. T. Parnell, N. R. Geraldi, B. B. Xu, G. G. Wells, S. Stuart-Cole, M. I. Newton, G. McHale, and D. Wood, "Low-friction self-centering droplet propulsion and transport using a Leidenfrost herringbone-ratchet structure," Phys. Rev. Appl. **11**, 034063 (2019).
[14]G. Dupeux, P. Bourrianne, Q. Magdelaine, C. Clanet, and D. Quéré, "Propulsion on a superhydrophobic ratchet," Sci. Rep. **4**, 5280 (2014).
[15]S. Shi, C. Ma, S. Hardt, and C. Lv, "Leidenfrost propulsion on symmetric textured surfaces via spontaneous symmetry breaking," Sci. Adv. **11**, eadt6677 (2025).
[16]Y. Guo, X. Liu, J. Ji, J. Wang, W. Sun, Z. Wang, K. Liu, and Y. Jia, "Singular ratchet-valley structure inducing droplet directional transport crossing all boiling states," Int. J. Heat Mass Transfer **245**, 127005 (2025).
[17]G. Lagubeau, M. Le Merrer, C. Clanet, and D. Quéré, "Leidenfrost on a ratchet," Nat. Phys. **7**, 395–398 (2011).
[18]G. Dupeux, T. Baier, V. Bacot, S. Hardt, C. Clanet, and D. Quéré, "Self-propelling uneven Leidenfrost solids," Phys. Fluids **25**, 051704 (2013).
[19]G. G. Wells, R. Ledesma-Aguilar, G. McHale, and K. Sefiane, "A sublimation heat engine," Nat. Commun. **6**, 6390 (2015).
[20]P. Agrawal, G. G. Wells, R. Ledesma-Aguilar, G. McHale, A. Buchoux, A. Stokes, and K. Sefiane, "Leidenfrost heat engine: Sustained rotation of levitating rotors on turbine-inspired substrates," Appl. Energy **240**, 399–408 (2019).
[21]H. Sugioka and S. Segawa, "Controllable Leidenfrost glider on a shallow water layer," AIP Adv. **8**, 115209 (2018).
[22]M. Shi, X. Ji, S. Feng, Q. Yang, T. J. Lu, and F. Xu, "Self-propelled hovercraft based on cold Leidenfrost phenomenon," Sci. Rep. **6**, 28574 (2016).
[23]A. Jonas, D. Orejon, and K. Sefiane, "Drag reduction and Leidenfrost effect on submerged ratcheted cylinder," Heat Transfer Eng. **44**, 2040–2061 (2023).
[24]A. Jonas, D. Orejon, and K. Sefiane, "Drag and instability of a free-falling cylinder in varying boiling regimes and with varying surface topographies," Chem. Eng. Res. Des. **192**, 239–252 (2023).
[25]I. U. Vakarelski, J. O. Marston, D. Y. Chan, and S. T. Thoroddsen, "Drag reduction by Leidenfrost vapor layers," Phys. Rev. Lett. **106**, 214501 (2011).
[26]I. U. Vakarelski, J. D. Berry, D. Y. Chan, and S. T. Thoroddsen, "Leidenfrost vapor layers reduce drag without the crisis in high viscosity liquids," Phys. Rev. Lett. **117**, 114503 (2016).
[27]I. U. Vakarelski, F. Kamoliddinov, A. Jetly, and S. T. Thoroddsen, "Leidenfrost spheres, projectiles, and model boats: Assessing the drag reduction by superhydrophobic surfaces," Colloids Surf., A **699**, 134573 (2024).
[28]I. U. Vakarelski, F. Kamoliddinov, A. Jetly, and S. T. Thoroddsen, "When superhydrophobicity can be a drag: Ventilated cavitation and splashing effects in hydrofoil and speed-boat models tests," Colloids Surf., A **628**, 127344 (2021).
[29]F. Kamoliddinov, I. U. Vakarelski, and S. T. Thoroddsen, "Hydrodynamic regimes and drag on horizontally pulled floating spheres," Phys. Fluids **33**, 093308 (2021).
[30]F. Kamoliddinov, I. U. Vakarelski, S. T. Thoroddsen, and T. T. Truscott, "Skipping under water: Buoyant sphere hydrodynamics at the air–water interface," Phys. Fluids **35**, 072106 (2023).
[31]A. Boomsma and F. Sotiropoulos, "Direct numerical simulation of sharkskin denticles in turbulent channel flow," Phys. Fluids **28**, 035106 (2016).
[32]D. Chen, Z. Shangguan, C. Sun, K. Zhang, W. Zhou, X. Liu, S. Hu, W. Yang, X. Liu, and H. Chen, "Biomimetic spanwise riblet coupled with hydrogel coating for drag reduction," Colloids Surf., A **728**, 138751 (2026).
[33]X. Feng, P. Sun, and B. Tian, "Recent developments of superhydrophobic surfaces (SHS) for underwater drag reduction opportunities and challenges," Adv. Mater. Interfaces **9**, 2101616 (2022).
[34]A. Jetly, I. U. Vakarelski, Z. Yang, and S. T. Thoroddsen, "Giant drag reduction on Leidenfrost spheres evaluated from extended freefall trajectories," Exp. Therm. Fluid Sci. **102**, 181 (2019).